Electronics Letters

LETTER OPEN ACCESS

Multistatic Synthetic Aperture Radar Autofocus for Back Projection Imaging of a Moving Target

Anmol Rattan[1] | Daniel Andre[1] | Mark Finnis[2]

[1]Centre for Electronic Warfare, Information and Cyber, Defence Academy of the United Kingdom, Cranfield University, Shrivenham, UK | [2]Centre for Defence Engineering, Cranfield University Defence Academy of the United Kingdom, Swindon, UK

Correspondence: Anmol Rattan (anmol.rattan@cranfield.ac.uk)

Received: 3 July 2024 | **Revised:** 31 January 2025 | **Accepted:** 5 March 2025

Funding: This research was supported by the Defence Science and Technology Laboratory (DSTL).

ABSTRACT

Synthetic Aperture Radar (SAR) plays a vital role in the surveillance of terrestrial and maritime targets, which are commonly in motion. As such, the ability to perform accurate real-time focusing and localisation on moving targets, particularly those moving with complex motion, is desired. Many existing autofocus algorithms struggle to achieve this and rely on sub-aperture processing of SAR data to estimate and compensate for phase errors attributed to unknown target motion. This paper presents a new metric-based autofocus approach, called Localised Threshold Sharpness (LTS), which employs multistatic SAR data to localise and focus a target moving with up to six degrees of freedom motion on a real-time, pulse-by-pulse basis. The algorithm is verified with experimental data, and its performance is compared against the performance of an existing measure of image sharpness suitable for pulse-by-pulse autofocusing, namely the intensity-squared metric, with varying levels of added noise. Normalised cross-correlation results demonstrate a resemblance of at least 80% between Multistatic SAR images focused via LTS autofocus and Multistatic SAR images ideally focused using target motion knowledge for signal-to-noise ratios above 3 dB.

1 | Introduction

Synthetic Aperture Radar (SAR) is widely used for remote sensing, including moving target detection and recognition [1]. The Back-Projection Algorithm (BPA) [2] leverages three-dimensional (3D) SAR trajectory knowledge for accurate imaging across various radar geometries and target scenes. However, phase errors from unknown target motion can degrade SAR images, posing challenges for autofocus techniques. Phase Gradient Autofocus (PGA) [3], including its generalised form for BPA imaging [4], struggles with space-variant phase errors. These errors arise from unaccounted range variations between moving target scatterers and the SAR platform, which can be significantly different across an image. Metric-based autofocus methods, such as intensity-squared, image contrast, and image entropy [5], have been applied to BPA, but only intensity-squared is suitable for pulse-by-pulse autofocus. However, it can misinterpret smeared images as focused due to its emphasis on high-intensity areas. Other sharpness metrics [6] and non-parametric techniques [7, 8] have been used to refocus moving targets, including those with unknown six degrees of freedom (6-DoF) motion. Yet, they are limited to post-processing and require multiple pulses to estimate phase errors, requiring patches or sub-images of unfocused images to identify target points to aid focusing. Consequently, achieving real-time, pulse-by-pulse autofocus and localisation of a target with complex, unknown motion remains an unsolved problem.

This paper introduces Localised Threshold Sharpness (LTS), a new metric-based autofocus method that utilises multistatic SAR measurements to perform joint real-time, pulse-by-pulse autofocus and localisation of targets moving with up to 6-DoF

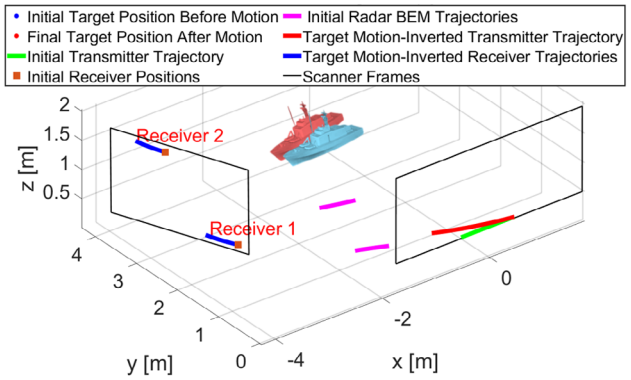

FIGURE 1 | Multistatic SAR geometry and target scene.

motion. It details the experimental setup for multistatic SAR measurements of a moving target and explains the LTS algorithm. Measurements were conducted using the Cranfield University Ground-Based SAR (GBSAR) system [9]. Focused SAR images using LTS and, for comparison, the intensity-squared metric [5] are presented and discussed.

2 | Multistatic Radar System and Target Scene

For a given bistatic configuration, the Cranfield University GBSAR system utilises a Vector Network Analyser (VNA) with ultra-wideband horn antennas for high-resolution bistatic SAR data collection. The transmitter and receiver, mounted on independent 2D scanners, move along separate vertical planes. The transmitter's rail spans 3.5 m in width and 1.45 m in height, while the receiver's rail measures 2.24 m by 1.45 m. Figure 1 illustrates the multistatic SAR geometry and target scene, showing the initial (blue) and final (red) positions of the laboratory ship model after motion. 6-DoF target motion refers to a rigid body moving in 3D space via linear translations (T_x, T_y, T_z) and axial rotations (roll (θ_x), pitch (θ_y), yaw (θ_z)). Target motion was emulated using the method described in [9], whereby theoretical motion was generated by appropriately transforming SAR trajectories. As such, all target scatterers moved by the same motion. For instance, if a SAR platform observes a target yaw by 10 degrees about its centre, equivalent data can be obtained by transforming the *initial SAR trajectory* to yaw by -10 degrees about this target centre while observing the stationary target. This transformed trajectory is called the *target motion-inverted SAR trajectory*. Since these radar trajectories, formed in simulation, were practically unattainable using the GBSAR scanner system due to the 2D scanner constraints, they were projected onto their respective 2D scanner windows along chords joining the target centre to trajectory positions. In simulation, *projected radar trajectory* coordinates were converted to local antenna axes coordinates as inputs for the laboratory scanning system. SAR measurements were acquired using the projected trajectories and a stationary ship model. Phase ramp corrections were applied to the data to compensate for range differences between target motion-inverted and projected trajectories, achieving phase data that would resemble measurements taken using the motion-inverted trajectories, thus enabling SAR measurements of a theoretically moving target. Target motion was modelled as uniform increments between pulses; the target concurrently completed -0.2 m, 0.15 m, and 0.1 m translations along the x, y, and z axes, and 5° roll, 2° pitch, and 10° yaw, over 100 pulses from rest. The initial Multistatic SAR geometry comprised two bistatic configurations, formed using two stationary receivers and a transmitter moving along a 1 m path. Repeating measurements with a single, coherent receiver at different locations rendered the combined collections equivalent to a single multiple-receiver multistatic collection. Data was collected using an 8–12 GHz frequency band for a 1.37 m ship model. Bistatic equivalent monostatic (BEM) trajectories (magenta) derived from the initial radar trajectories [10] resulted in azimuth angles of 7.1° and 7.4° and average bistatic angles of 54.8° and 72.2° for receivers 1 and 2, respectively. This produced theoretical average bistatic range resolutions of ~4.2 cm and ~4.6 cm and cross-range resolutions of ~13.6 cm and ~14.4 cm at ranges of ~4.1 m and ~4.2 m from the target centre for receivers 1 and 2, respectively.

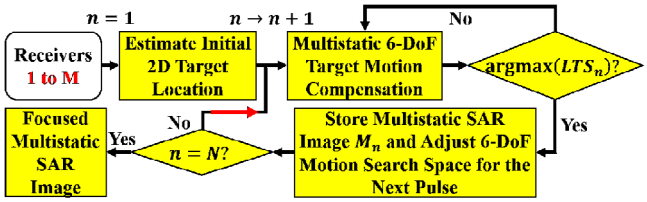

FIGURE 2 | Overview of LTS autofocus.

3 | LTS Autofocus

Figure 2 provides an overview of the proposed autofocus method. LTS autofocus optimises target motion estimation and bistatic SAR trajectory adjustments on a pulse-by-pulse basis to generate a focused multistatic SAR image, where target signature intensity is concentrated around estimated 2D target scatterers. For each pulse P_n, where n is the pulse number, the mean of intensity-normalised range profiles for P_1 of each receiver r $\{r = 1, \ldots, M\}$ estimates the initial bistatic radar-to-target range ($d_{r,n}$). The initial 2D target location is then determined via multilateration [11]. To enhance robustness against noise, only range profiles with normalised intensities at or above the half-power point (-3 dB) are considered. Spatial coordinates of an arbitrary point in 3D space are defined as $\boldsymbol{a} = (x, y, z)$. Acknowledging $d_{r,n}$ to be an estimation rather than an exact range to a single target scatterer $\boldsymbol{a}_n$ that represents the general location of the target using range profiles of pulse n, location of $\boldsymbol{a}_n$ can be hypothesised using the absolute residual bistatic range ($\delta b_{r,n}$), defined as the absolute difference between $d_{r,n}$ and the total bistatic distance between possible locations of $\boldsymbol{a}_n$ and known positions of transmitter $\boldsymbol{p}_{t,n}$ and a receiver $\boldsymbol{p}_{r,n}$:

$$\delta b_{r,n} = \left|\left|p_{t,n} - a_n\right| + \left|a_n - p_{r,n}\right| - d_{r,n}\right| \tag{1}$$

The 2D location of the target scatterer $\boldsymbol{a}_n$ on a given imaging plane can be estimated by minimising the sum of the absolute residual bistatic ranges of all receivers in the multistatic system to a 2D target point defined as:

$$\widehat{\boldsymbol{a}_n} = \text{argmin}\left\{\sum_r \left(\delta b_{r,n}\right)\right\} \tag{2}$$

Let the BPA SAR image formed from the range profiles for all receivers, for only the n^{th} pulse, be denoted L_n, which we will refer to as a single-pulse SAR image. Let M_n denote the coherent sum of single-pulse SAR images from P_1 to P_n from all receivers:

$$M_n = \sum_{k=1}^{n} L_k \tag{3}$$

$L_1 = M_1$ is to be used as a reference image. Pulse-by-pulse searches for estimating 6-DoF target motion values and transforming bistatic SAR trajectories accordingly to produce a focused multistatic SAR image are conducted. During autofocus, the target and its location are assumed to be unknown. Hence, estimation of rotational motion values (roll, pitch and yaw) is performed about $\boldsymbol{a}_1$, which would, ideally, result in equivalent rotations to those by the target about its target centre. Transformation of known transmitter $\boldsymbol{p}_{t,n}$ and receiver $\boldsymbol{p}_{r,n}$ coordinates for a given pulse P_n after P_1 $\{n = 2, \ldots, N\}$ can be defined as:

$$\boldsymbol{p}_{t_{n(new)}} = \left(\boldsymbol{R}_n^{-1}\left(\boldsymbol{p}_{t_n} - \boldsymbol{a}_1\right)\right) + \boldsymbol{T}_n \tag{4}$$

$$\boldsymbol{p}_{r_{n(new)}} = \left(\boldsymbol{R}_n^{-1}\left(\boldsymbol{p}_{r_n} - \boldsymbol{a}_1\right)\right) + \boldsymbol{T}_n \tag{5}$$

where $\boldsymbol{p}_{t_{n(new)}}$ and $\boldsymbol{p}_{r_{n(new)}}$ are new coordinates of the transmitter and receiver r after 6-DoF transformations from initial positions ($\boldsymbol{p}_{t_n}$ and $\boldsymbol{p}_{r_n}$) for a given pulse P_n, respectively. These 6-DoF transformations for each pulse P_n consist of $\boldsymbol{T}_n$, which represents estimated translations (T_x, T_y, T_z) by the target along all three orthogonal axes, and $\boldsymbol{R}_n$, which is a rotation matrix with estimated axial rotations (θ_x, θ_y, θ_z) of the target about $\boldsymbol{a}_1$. For a given pulse P_n after P_1, LTS defines the quality of focus of a sub-aperture multistatic SAR image as:

$$\text{LTS}_n = \frac{I_{n,max}}{\left(\left(\sum_{(i,j)\in W}\left|I_{n(i,j)}\right|^2 - I_{n,max}\right) + \zeta\left|\boldsymbol{a}_{n-1} - \boldsymbol{a}_n\right|\right)} \tag{6}$$

$$\left(\widehat{\boldsymbol{T}_n}, \widehat{\boldsymbol{\theta}_n}\right) = \text{argmax}\left\{\text{LTS}_n\left(\boldsymbol{T}_n, \boldsymbol{\theta}_n\right)\right\} \tag{7}$$

where W is a window centred around a pixel with maximum intensity $I_{n,max}$ of the multistatic SAR image M_n, $I_{n(i,j)}$ is the intensity of a pixel located at row i and column j of the windowed image, and ζ is a weighting factor that governs the impact of location consistency.

4 | Optimisation

Optimisation of 2D target scatter and 6-DoF target motion estimates, as described in Equations (2) and (7), was performed using Particle Swarm (PS) optimisation, which is well-suited for multi-dimensional search problems [12]. Following optimal maximisation of LTS_n $\{n = 2, \ldots, N\}$, estimated $\boldsymbol{T}_n$ and $\boldsymbol{\theta}_n$ values and corresponding focused multistatic SAR images M_n are stored. Autofocus iterations continue until n reaches the total number of pulses N, resulting in a fully focused multistatic SAR image. In each iteration, only a single-pulse multistatic image L_n is newly generated and coherently added to M_{n-1} to form multistatic SAR image M_n. To ensure accuracy and avoid being trapped at local optima, PS optimisation was designed with appropriate search space bounds, swarm particle count, and iteration limits. Parallel processing was applied to BPA SAR imaging and PS optimisation, reducing computational burden. Application of the LTS autofocus algorithm to motion models other than 6-DoF motion and more efficient SAR imaging techniques is beyond this paper's scope.

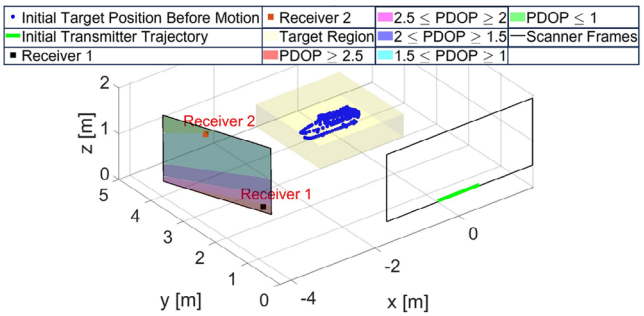

FIGURE 3 | Areas of Position Dilution of Precision (PDOP) values to aid with the positioning of receiver 2 for target localisation.

5 | Multistatic Radar Geometry Limitations

The accuracy of target localisation as part of LTS autofocus depends on the geometry between the transmitter, receivers and target, which can be assessed using the position dilution of precision (PDOP) [13]. PDOP can be defined as:

$$\text{PDOP} = \sqrt{\text{Tr}\left(\left(\boldsymbol{H}^{\text{T}}\boldsymbol{H}\right)^{-1}\right)} \tag{8}$$

where $\boldsymbol{H}$ is the Jacobian matrix (also known as the geometry matrix) derived from the line-of-sight (LOS) vectors from each BEM trajectory to the target. Tr refers to the trace of the matrix. Achieving the lowest possible PDOP is optimal; PDOP values between 1 and 2 represent excellent confidence in the accuracy of SAR measurements used to locate a target. Beginning with the initial transmitter trajectory and position of receiver 1 in this study, Figure 3 shows areas of the receiver scanner frame—denoted by ranges of PDOP values—which can be used to position receiver 2 to aid the localisation of points within the target region (yellow) enclosing the laboratory ship model (blue). Situated at a position that results in PDOP ≅1.3, the position of receiver 2 in this study can be considered suitable for the localisation of the laboratory ship model.

6 | Experimental Results

The Multistatic SAR image of the laboratory ship model was autofocused on a pulse-to-pulse basis via LTS maximisation. For comparison, autofocus was also conducted by maximising the intensity-squared metric [5]—replacing LTS_n in Equation (7) with S_n:

$$S_n = \sum_{(i,j)\in W}\left|I_{n(i,j)}\right|^2 \tag{9}$$

For LTS autofocus in this study, W was a $2m \times 2m$ window and ζ had a fixed value of 0.07. Multistatic SAR images autofocused with different values of ζ were compared with an image

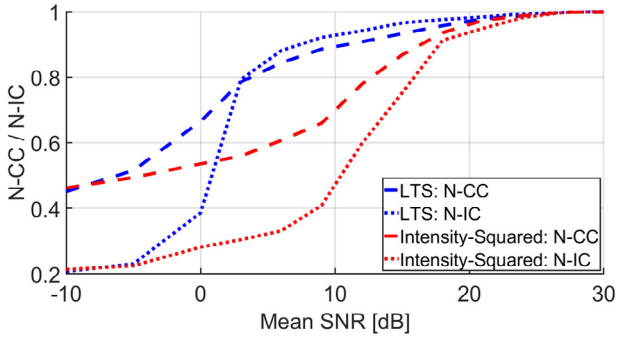

FIGURE 4 | Normalised Cross-Correlation (N-CC) and Normalised Image Contrast (N-IC) results.

ideally focused using true target motion. Their normalised cross-correlation results suggested that ζ values within 0.05 and 0.1 provide a good balance of allowing minor changes between estimated target locations—possibly due to different viewing angles between pulses—and enhancing focus. Note that Equations (7) and (9) represent two different optimisation problems: L1-norm and L2-norm respectively, where Equation (7) prioritises absolute deviations and Equation (9) emphasises squared deviations. To ensure consistency across both PS optimisations, identical swarm initialisation, velocity updates, constraints and parameters were applied. This included using the same number of particles, iterations, inertia weight and acceleration coefficients for both optimisations. Particles started from the same positions and updated their positions identically within the same 6-DoF motion search space for each optimisation. Image contrast and normalised cross-correlation with an ideally focused multistatic SAR image were evaluated to compare the performance of multistatic SAR image autofocusing via the LTS and the intensity-squared metrics. Image contrast (IC) [5] is defined as:

$$\mathrm{IC} = \frac{\sqrt{\mathrm{A}\left\{\left[I(x,y) - \mathrm{A}\{I(x,y)\}\right]^2\right\}}}{\mathrm{A}\{I(x,y)\}} \tag{10}$$

where the operator $A\{\}$ represents the spatial mean over the image coordinates (x, y) and I is the image intensity. A well-focused image is considered to have a high contrast. Phase history data was contaminated with additive white noise to test the robustness of each autofocus metric against noise. Figure 4 shows normalised cross-correlation (N-CC) and normalised image contrast (N-IC) results of multistatic SAR images autofocused using the LTS and intensity-squared metrics, respectively, for a range of mean signal-to-noise ratios (SNRs). Figure 5 shows multistatic SAR images formed using measurements by receivers 1 and 2 for all 100 pulses, which are (a) ideally focused, (b) unfocused, (c) autofocused using the LTS and (d) intensity-squared metrics, for a mean SNR of 10 dB.

N-CC and N-IC results seen in Figure 4 reveal better autofocusing by the LTS metric than the intensity-squared metric for mean SNRs between 0 dB and 25 dB. The LTS metric significantly outperforms the intensity-squared metric for mean SNRs above 3 dB; autofocus becomes difficult below 3 dB SNR, as the presence of noise becomes excessive for reliable target location and signature identification. Figure 5 also supports the utility of the LTS metric, as the multistatic SAR image autofocused using

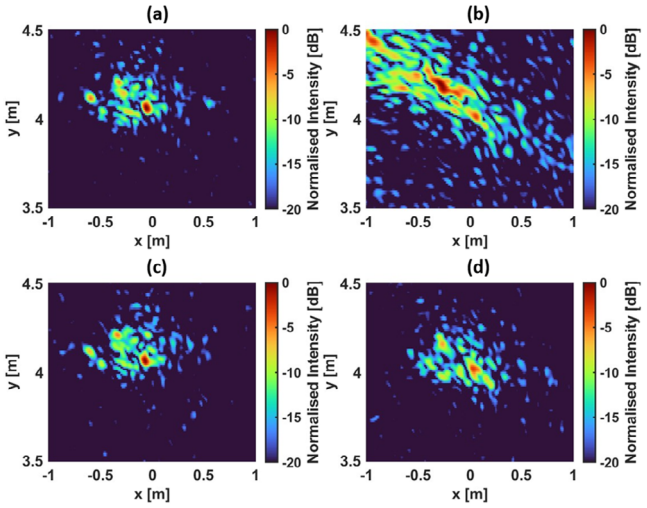

FIGURE 5 | Multistatic SAR images, for a mean SNR of 10 dB: (a) Ideally focused, (b) Unfocused, (c) Autofocused using the LTS metric and (d) Intensity-Squared metric.

the LTS metric in Figure 5(c) bares a closer resemblance to the ideally focused multistatic SAR image in Figure 5(a).

7 | Conclusion

A new metric-based autofocus algorithm, LTS autofocus, capable of using multistatic measurements for 6-DoF, real-time, target motion compensation on a pulse-by-pulse basis, has been presented. The LTS metric showed improved autofocusing compared to the intensity-squared metric, an existing image sharpness metric suitable for pulse-by-pulse autofocus, for mean SNRs between 3 dB and 25 dB. This study considered a single target; for target SNRs above 3 dB, good autofocus results can be expected in more complex scenarios. However, other objects in the SAR image, including clutter, may appear defocused due to SAR trajectory transformations not accounting for all object movements. Sub-Image processing to identify target regions may help. The experimental setup in this study resembled an ideal scenario, where measurements of a scale model with theorised motion in an anechoic chamber using a 'stop-and-shoot' method were made. Future work will enhance efficiency and robustness, extending the algorithm to more realistic and complex scenarios with additional multistatic receivers for improved multi-target autofocus and localisation.

Author Contributions

Anmol Rattan: conceptualisation, data curation, formal analysis, investigation, methodology, software, validation, visualisation, writing – original draft, writing – review and editing. **Daniel Andre**: conceptualisation, funding acquisition, investigation, methodology, project administration, software, supervision, writing– review and editing. **Mark Finnis**: resources and software.

Acknowledgements

This work was funded by Defence Science and Technology Laboratory.

Conflicts of Interest

The authors declare no conflict of interest.

Data Availability Statement

SAR data is the subject of ongoing research but may be made available on request to the corresponding author or the Cranfield GBSAR group.

References

1. M. Martorella, *Multidimensional Radar Imaging*, 1 (SciTech Publishing, 2019).

2. L. A. Gorham and L. J. Moore, "SAR Image Formation Toolbox for MATLAB," *Proceedings of SPIE* 7699 (2010): 855375.

3. D. E. Wahl, P. H. Eichel, D. C. Ghiglia, and C. V. Jakowatz, "Phase Gradient Autofocus-a Robust Tool for High Resolution SAR Phase Correction," *IEEE Transactions on Aerospace and Electronic Systems* 30, no. 3 (1994): 827–835.

4. A. Evers and J. A. Jackson, "A Generalized Phase Gradient Autofocus Algorithm," *IEEE Transactions on Computational Imaging* 5, no. 4 (2019): 606–619.

5. A. Sommer and J. Ostermann, "Backprojection Subimage Autofocus of Moving Ships for Synthetic Aperture Radar," *IEEE Transactions on Geoscience and Remote Sensing* 57, no. 11 (2019): 8383–8393.

6. J. Fienup, "Detecting Moving Targets in SAR Imagery by Focusing," *IEEE Transactions on Aerospace and Electronic Systems* 37, no. 3 (2001): 794–809, https://doi.org/10.1109/7.953237.

7. S. Werness, W. Carrara, L. Joyce, and D. Franczak, "Moving Target Imaging Algorithm for SAR Data," *IEEE Transactions on Aerospace and Electronic Systems* 26, no. 1 (1990): 57–67, https://doi.org/10.1109/7.53413.

8. D. A. Garren, "Theory of Arbitrary Rigid Object Motion Autofocus for Non-Uniform Target Rotation and Translation," *IET Radar Sonar & Navigation* 14, no. 11 (2020): 1803–1814, https://doi.org/10.1049/iet-rsn.2020.0201.

9. A. Rattan, D. Andre, and M. Finnis, "Multistatic Hybrid SAR/ISAR Data Generation Using a Stationary Target," in *Proceedings of the International Conference on Radar Systems (RADAR 2022)*, 2022,71–76.

10. M. Martorella, D. Cataldo, and S. Brisken, "Bistatically Equivalent Monostatic Approximation for Bistatic ISAR", in *Proceedings of the IEEE Radar Conference (RadarCon)*, 2013, 1–5.

11. Brisken, S. M. Martorella, T. Mathy, C. Wasserzier, J. G. Worms, and J. H. G. Ender, "Motion Estimation and Imaging with a Multistatic ISAR System," *IEEE Transactions on Aerospace and Electronic Systems* 50, no. 3 (2014): 1701–1714.

12. J. Kennedy and R. C. Eberhart, "A Discrete Binary Version of the Particle Swarm Algorithm," in *Proceedings of the 1997 IEEE International Conference on Systems, Man, and Cybernetics. Computational Cybernetics and Simulation*, 5, 1997, 4104–4108.

13. E. Kaplan and C. Hegarty, *Understanding GPS—Principles and Applications*, 2nd ed. (Artech House, 2006).

Multistatic synthetic aperture radar autofocus for back projection imaging of a moving target

Rattan, Anmol

2025-01

Rattan A, Andre D, Finnis M. (2025) Multistatic synthetic aperture radar autofocus for back projection imaging of a moving target. Electronics Letters, Volume 61, Issue 1, January/December 2025, Article number e70217

https://doi.org/10.1049/ell2.70217